Journal of Sound and Vibration 329 (2010) 3507–3519

Contents lists available at ScienceDirect

Journal of Sound and Vibration

journal homepage: www.elsevier.com/locate/jsvi

Dynamical behaviors of a plate activated by an induction motor

D.O. Tcheutchoua Fossi, P. Woafo *

Laboratory of Modelling and Simulation in Engineering and Biological Physics and TWAS Research Unit, Department of Physics, Faculty of Science, University of Yaoundé I, P.O. Box 812, Yaoundé, Cameroon

ARTICLE INFO

Article history:
Received 23 December 2009
Received in revised form
13 March 2010
Accepted 13 March 2010
Handling Editor: L.N. Virgin

ABSTRACT

Dynamics and chaotification of a system consisting of an induction motor activating a mobile plate (with variable contents) fixed to a spring are studied. The dynamical model of the device is presented and the electromechanical equations are formulated. The oscillations of the plate are analyzed through variations of the following reliable control parameters: phase voltage supply of the motor, frequency of the external source and mass of the plate. The dynamics of the system near the fundamental resonance region presents jump phenomenon. Mapping of the control parameters planes in terms of types of motion reveals period-*n* motion, quasi-periodicity and chaos. Anti-control of chaos of the induction motor is also obtained using the field-oriented control associated to the time delay feedback control.

1. Introduction

Asynchronous motor (AS motor) named against induction motors is a class of electromechanical system where nonlinear dynamics is very interesting. They are widely used in various industrial modern processes due to their relatively low cost, low maintenance, high robustness and reliability. In order to avoid the undesirable phenomena such as locking, coughs and sputters in the AS motors and to regulate its main variables (current, flux, speed and torque) to their reference values, many investigations have been recently carried out based on the vectorial control strategy [1–4], on the control by input–output linearization [5–8] and on the direct torque control [9]. From the beginning of 1990s, a number of researches on chaos in vibrational systems have been undertaken: on identification of chaos [10–13], on the avoidance of chaos [14,15], stabilization and synchronization [16,17], control and anti-control of chaos [18–20], control of vibration [21]. Nonlinear dynamics of electromechanical systems with translational or pendulum-arm has been studied extensively in recently [22–24]. These studies have been guided by the fact that chaos is useful and beneficial in some niche applications such as chaotic industrial shakers [25], chaotic monitoring and compaction [26,27], and industrial mixing processes [28,29].

The electromechanical system proposed in this paper is an extension of one use in [12,30]. It consists of a mobile plate with variable contents, fixed to a spring and activated by an induction motor. Knowing that the AS motor is inherently nonlinear in its natural functioning, the purpose of this work is to capitalize that nonlinearity and the other ones in the device for generation of several interesting phenomena such as jump, period-*n*, quasi-periodicity and chaotic motions. Moreover, we generate the desired chaos in the system using the field-oriented control associated to the time delay feedback control. The technological interest of this study is to optimize the efficiency of the device designing it with a large range of desired dynamical behaviors obtained varying control parameters. The device can be used in various branches of electromechanical engineering for domestic appliances, industrial food processing, mining and sandpit in sieving or sifting processes.

* Corresponding author.
E-mail address: pwoafo1@yahoo.fr (P. Woafo).

0022-460X/$ - see front matter © 2010 Elsevier Ltd. All rights reserved.
doi:10.1016/j.jsv.2010.03.017

Section 2 presents the description of the model and its electromechanical equations. Section 3 analyses the dynamical behavior of the system, Section 4 is devoted to anti-control of chaos in the device and Section 5 concludes the work.

2. Electromechanical device and equations

The device in Fig. 1 consists of a mobile plate with variable contents fixed to a spring and activated by an induction motor. The AS motor used is a three-phase one with two parts: a stator (inductor) and a rotor mobile around a revolution axis. The electromagnetic torque which is produced by the electromotor is transmitted to the plate by the connecting-track rod system which is mechanically fixed to the rotor. The system parameters values are given in Tables 1 and 2.

In the continuation, the following assumptions will be considered: unsaturated magnetic circuit, negligible magnetic hysteresis, negligible magnetic flux leak, negligible torque due to dry frictions and negligible variation of the rotor resistance. The three-phase AS motor is generally modeled in the turning reference frame (d–q) where d is the direct axis and q the quadrature axis or in the stator fixed frame (α–β) (see Fig. 2a) [4]. The electromechanical equations of AS motor are written here in the frame (d–q) because it is most general. The reference frame transformation and the dynamical equivalent diagram of AS motor in the frame (d–q) are given in Figs. 2a and 2b.

In Fig. 2a, θ_s and θ_r are the electrical angles in the frames (α_s–d) and (α_r–d), respectively. θ is the angular displacement of rotor and ω its mechanical velocity. ω_s is the angular velocity of d, q-axis in the stator reference frame. The stator and rotor voltage equations given by Kirchhoff's law (see Fig. 2b) are written as

$$\underline{u_s} = R_s \underline{i_s} + \mathrm{d}\frac{\underline{\phi_s}}{\mathrm{d}t} + \mathrm{j}\frac{\mathrm{d}\theta_s}{\mathrm{d}t}\underline{\phi_s} \tag{1a}$$

$$\underline{u_r} = 0 = R_r \underline{i_r} + \mathrm{d}\frac{\underline{\phi_r}}{\mathrm{d}t} + \mathrm{j}\frac{\mathrm{d}\theta_r}{\mathrm{d}t}\underline{\phi_r} \tag{1b}$$

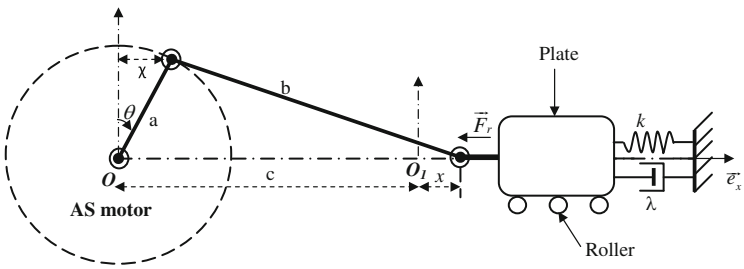

Fig. 1. Electromechanical device.

Table 1
Parameters of the AS motor system.

Parameter	Value	Unit
Stator resistance: R_s	9.65	Ω
Rotor resistance: R_r	4.3047	Ω
Stator inductance: L_s	0.4718	H
Rotor inductance: L_r	0.4718	H
Mutual inductance: L_{sr}	0.4475	H
Rotor inertia: J_r	0.00293	kg m^2
Viscous friction coefficient: C_V	0.038	N m s/rad
Number of pole pairs: n_p	2	

Table 2
Parameters of the plate and spring.

Parameter	Value	Unit
Mass of the plate: m_p	Variable	kg
Viscous damping: λ	25.0	N s/m
Stiffness coefficient: k	3500.0	N/m

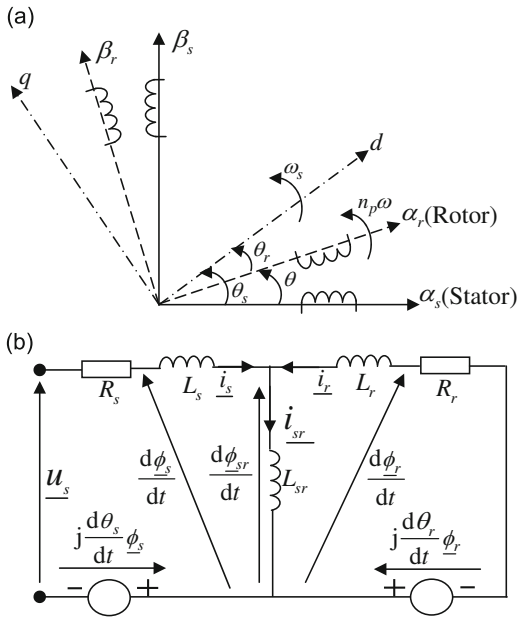

Fig. 2. (a) Reference frame transformation and (b) dynamical equivalent diagram of AS Motor in the frame (d–q).

where j is the imaginary number:

$$\underline{\phi_s} = L_s\underline{i_s} + L_{sr}\underline{i_r} \tag{2a}$$

$$\underline{\phi_r} = L_r\underline{i_r} + L_{sr}\underline{i_s} \tag{2b}$$

and

$$\frac{d\theta_r}{dt} = \frac{d\theta_s}{dt} - \frac{d\theta}{dt} = \omega_s - n_p\omega \tag{3}$$

The projection of Eqs. (1) and (2) on d, q-axis in a synchronous frame give the stator and rotor voltage equations of the induction motor which can be expressed as follows:

$$u_{sd} = R_s i_{sd} + \frac{d\phi_{sd}}{dt} - \omega_s\phi_{sq} \tag{4a}$$

$$u_{sq} = R_s i_{sq} + \frac{d\phi_{sq}}{dt} + \omega_s\phi_{sd} \tag{4b}$$

$$u_{rd} = 0 = R_r i_{rd} + \frac{d\phi_{rd}}{dt} - (\omega_s - n_p\omega)\phi_{rq} \tag{4c}$$

$$u_{rq} = 0 = R_r i_{rq} + \frac{d\phi_{rq}}{dt} + (\omega_s - n_p\omega)\phi_{rd} \tag{4d}$$

with

$$\phi_{sd} = L_s i_{sd} + L_{sr} i_{rd} \tag{5a}$$

$$\phi_{sq} = L_s i_{sq} + L_{sr} i_{rq} \tag{5b}$$

$$\phi_{rd} = L_r i_{rd} + L_{sr} i_{sd} \tag{5c}$$

$$\phi_{rq} = L_r i_{rq} + L_{sr} i_{sq} \tag{5d}$$

where i_{sq} and i_{sd} are the stator armature currents, u_{sq} and u_{sd} the stator voltages and ϕ_{rq} and ϕ_{rd} the rotor fluxes, on the q- and d-axis reference frame, respectively. Eqs. (4) can be written taking into account Eqs. (5) as follows:

$$\sigma L_s \frac{\mathrm{d}i_{sd}}{\mathrm{d}t} + \left(R_s + \frac{L_{sr}^2}{T_r L_r}\right) i_{sd} - \omega_s \sigma L_s i_{sq} - \frac{L_{sr}}{T_r L_r}\phi_{rd} - n_p \frac{L_{sr}}{L_r}\omega\phi_{rq} = u_{sd} \tag{6a}$$

$$\sigma L_s \frac{\mathrm{d}i_{sq}}{\mathrm{d}t} + \omega_s \sigma L_s i_{sd} + \left(R_s + \frac{L_{sr}^2}{T_r L_r}\right) i_{sq} + n_p \frac{L_{sr}}{L_r}\omega\phi_{rd} - \frac{L_{sr}}{T_r L_r}\phi_{rq} = u_{sq} \tag{6b}$$

$$\frac{\mathrm{d}\phi_{rd}}{\mathrm{d}t} + \frac{1}{T_r}\phi_{rd} - \frac{L_{sr}}{T_r} i_{sd} - (\omega_s - n_p\omega)\phi_{rq} = 0 \tag{6c}$$

$$\frac{\mathrm{d}\phi_{rq}}{\mathrm{d}t} + \frac{1}{T_r}\phi_{rq} - \frac{L_{sr}}{T_r} i_{sq} + (\omega_s - n_p\omega)\phi_{rd} = 0 \tag{6d}$$

where $T_r = L_r/R_r$ is the rotor time constant, $\sigma = 1-(L_{sr}^2/L_r L_s)$ the dispersion coefficient. When the AS motor is connected to a three phases power system of frequency f and phase voltage amplitude v, the corresponding u_{sd} and u_{sq}, applying Park's transformation, are expressed as [4,31]

$$u_{sd} = v\sqrt{3}\cos(2\pi f t - \theta_s) \tag{7a}$$

$$u_{sq} = v\sqrt{3}\sin(2\pi f t - \theta_s) \tag{7b}$$

where $\theta_s = \int \omega_s \,\mathrm{d}t$ and $\omega_s = 2\pi f/n_p$.

The dynamical equation of the rotor is

$$J_r \frac{\mathrm{d}\omega}{\mathrm{d}t} + C_v\omega = T_e + T_L \tag{8}$$

where T_e is the electromagnetic torque due to the Laplace force and T_L the load torque.

The electromagnetic torque developed by the induction motor is expressed as [2,4,31]

$$T_e = n_p \frac{L_{sr}}{L_r}(\phi_{rd} i_{sq} - \phi_{rq} i_{sd}) \tag{9}$$

The relationship between T_L and F_r (resistance force of the plate) is written as

$$T_L \,\mathrm{d}\theta = -F_r \,\mathrm{d}x \tag{10}$$

and the load torque can be expressed as

$$T_L = -F_r \frac{a\cos\theta}{1-\varepsilon\sin\theta} \tag{11}$$

where $F_r = \lambda(\mathrm{d}x/\mathrm{d}t) + kx$ and $\varepsilon = a/(x+c)$ which is generally a small quantity due to the fact that a and x are smaller than c. a is the track rod length, x the displacement of the plate and c the distance between points 0 and 0_1. The dynamical equation of the plate is written as

$$m_p \frac{\mathrm{d}^2x}{\mathrm{d}t^2} = -F_r + F_m \tag{12}$$

where m_p is the mass of the plate and F_m the motive force induced by the electromotor. The motive force F_m is expressed as

$$F_m = \lambda \frac{\mathrm{d}\chi}{\mathrm{d}t} + k\chi = n_p\lambda a\omega\cos\theta + ka\sin\theta \tag{13}$$

Eq. (12) can be written taking into account Eq. (13) as follows:

$$m_p \frac{\mathrm{d}^2x}{\mathrm{d}t^2} + \lambda\frac{\mathrm{d}x}{\mathrm{d}t} + kx - n_p\lambda a\omega\cos\theta - ka\sin\theta = 0 \tag{14}$$

Denote

$$\cdot = \frac{\mathrm{d}}{\mathrm{d}\tau}, \quad \cdot\cdot = \frac{\mathrm{d}^2}{\mathrm{d}\tau^2}, \quad \omega_0 = \sqrt{\frac{k}{m_p}} = 2\pi f_0, \quad \tau = \omega_0 t, \quad y_1 = \frac{i_{sd}}{i_0}$$

$$y_2 = \frac{i_{sq}}{i_0}, \quad \Phi_1 = \frac{\phi_{rd}}{\varphi_0}, \quad \Phi_2 = \frac{\phi_{rq}}{\varphi_0}, \quad \Omega = \frac{\omega}{\omega_0}, \quad z = \frac{x}{a}, \quad \varpi = \frac{2\pi f}{\omega_0} = \frac{f}{f_0} \tag{15}$$

and

$$\gamma = \frac{R_s}{\sigma L_s} + \frac{L_{sr}^2}{\sigma T_r L_s L_r}, \quad \kappa = \frac{L_{sr}}{\sigma L_s L_r}, \quad a_1 = \frac{\gamma}{\omega_0}, \quad a_2 = \frac{\kappa\varphi_0}{T_r\omega_0 i_0}, \quad a_3 = \frac{1}{\omega_0 T_r}, \quad a_4 = \frac{L_{sr} i_0}{\omega_0\varphi_0 T_r}$$

$$E=\frac{v\sqrt{3}}{\sigma L_s\omega_0 i_0},\quad \chi_E=\frac{\kappa\varphi_0}{i_0},\quad \chi_T=\frac{n_pL_{sr}\varphi_0 i_0}{L_rJ_r\omega_0^2},\quad \eta=\frac{\lambda}{m_p\omega_0},\quad \eta_1=\frac{\lambda a^2}{J_r\omega_0},\quad \eta_2=\frac{ka^2}{J_r\omega_0^2},\quad \mu=\frac{C_V}{J_r\omega_0} \tag{16}$$

Replacing Eqs. (15) and (16) into Eqs. (6), (8) and (14), taking into account Eqs. (7), (9), (11) and (14), one obtains the following set of dimensionless differential equations:

$$\dot{y}_1+a_1y_1-y_2\varpi/n_p-a_2\Phi_1-n_p\chi_E\Omega\Phi_2=E\cos(\varpi(1-1/n_p)\tau) \tag{17a}$$

$$\dot{y}_2+a_1y_2+y_1\varpi/n_p-a_2\Phi_2+n_p\chi_E\Omega\Phi_1=E\sin(\varpi(1-1/n_p)\tau) \tag{17b}$$

$$\dot{\Phi}_1+a_3\Phi_1-a_4y_1-(\varpi/n_p-n_p\Omega)\Phi_2=0 \tag{17c}$$

$$\dot{\Phi}_2+a_3\dot{\Phi}_2-a_4y_2+(\varpi/n_p-n_p\Omega)\Phi_1=0 \tag{17d}$$

$$\dot{\theta}=n_p\Omega \tag{17e}$$

$$\dot{\Omega}+\mu\Omega=\chi_T(\Phi_1y_2-\Phi_2y_1)-(\eta_1\dot{z}+\eta_2z)\frac{\cos\theta}{1-\varepsilon\sin\theta} \tag{17f}$$

$$\ddot{z}+\eta\dot{z}+z-n_p\eta\Omega\cos\theta-\sin\theta=0 \tag{17g}$$

3. Dynamical behavior of the device

3.1. Oscillatory states

Eqs. (17) present in the absence of the input voltage a single stationary point $(x_1,x_2,y_1,y_2,\Phi_1,\Phi_2,\theta,\Omega,\dot{z},z)=(0,0,0,0,0,0,0,0)$ which is asymptotically stable. The aim of this subsection is to use the fourth order Runge–Kutta algorithm with constant time step to solve numerically the non-dimensional differential equations (17) to find the behavior of the dimensionless maximum amplitude of plate vibration. In Fig. 3, the frequency–response diagram [12] is plotted in terms of the dimensionless displacement z and the control parameter is the dimensionless frequency of the three phases power system ϖ. This resonance curve shows similar results when the normalized frequency of the three phases power system ϖ is slowly increased or decreased. As ϖ increases from 0 to 5.0, the maximum response amplitude increases from 1.0 to 1.15 and then decreases to 1.04 and increases again to 1.278. Then it jumps from 1.28 to 2.94, decreases and increases further to a maximum value 3.887 and then decreases to 0.54.

3.2. Chaotic behavior

As the plate content could vary, the mass m_p is taken as a reliable control parameter in this subsection. The aim here is to use the fourth order Runge–Kutta algorithm to solve numerically Eqs. (17) and mark the regions where the system shows period-n motion, quasi-periodicity and chaos. For identifying these states, the dynamical behavior is derived using the bifurcation diagram varying the frequency f at a fixed phase amplitude v (frequency scanning) at one hand, and varying

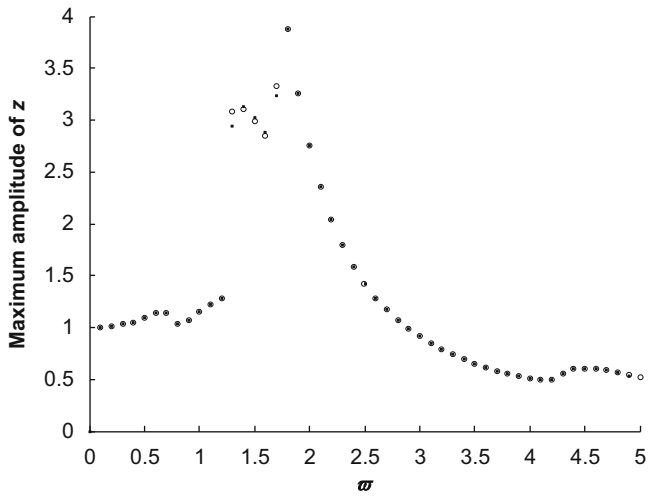

Fig. 3. Maximum amplitude of plate as function of the normalized frequency with the parameters of Tables 1 and 2 and $v=102.9$ V, $m_p=2.0$ kg, $a=0.1$ m, $\varepsilon=0.15$, $\varphi_0=1$ Wb, $i_0=1$ A, $f_0=6.658$ Hz.

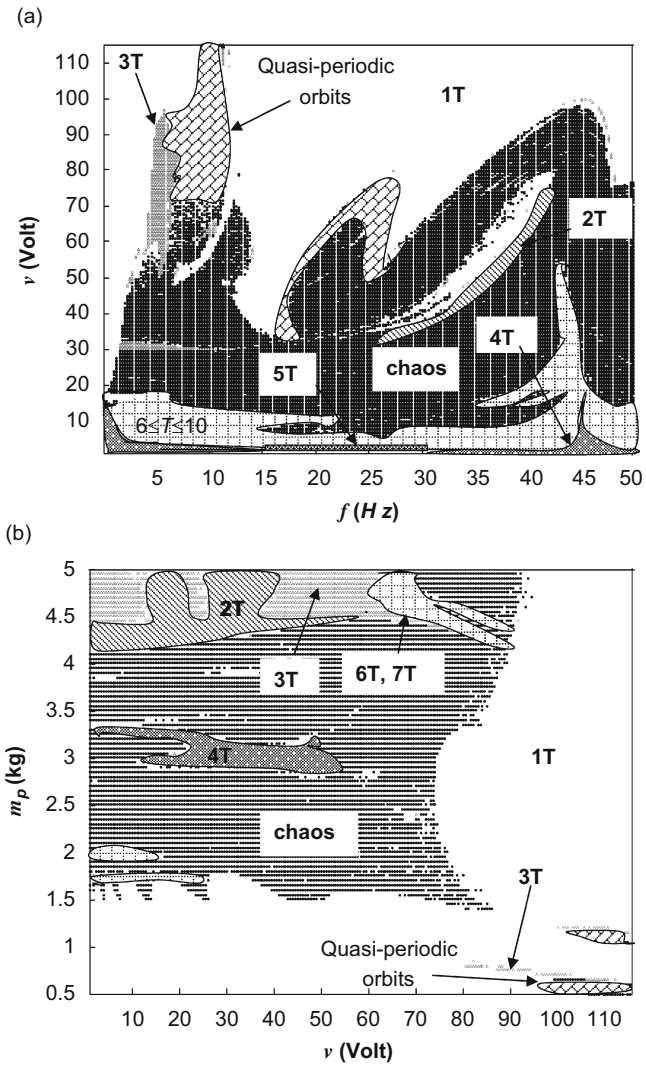

Fig. 4. Regions of different behaviors exhibited by the plate with the parameters of Fig. 3. (a) m_p=2.0 kg and f_0=6,658 Hz; and (b) f=50.0 Hz.

the amplitude v at a fixed mass of the plate m_p (amplitude scanning) on the other hand. Resulting phase diagrams in the $v-f$ plane and in the m_p-v plane are shown in Figs. 4a and b, respectively. One observes that the device exhibits some large domains of periodic oscillations and chaotic motions. However, there are small windows of quasi-periodicity motion and period-nT ($2 \le n \le 10$) oscillations. In Fig. 4a, for low v values < 5.72 V and f values in the region $0 \le f \le 50$ Hz, period-nT ($4 \le n \le 10$) oscillations occur. When v increases ($v > 5.72$ V), the transition from period-nT oscillations to chaos occurs. As the forcing parameter v increases further, the system exhibits quasi-periodicity and chaotic motions, period-2T and period-3T oscillations. When the value of v exceeds a certain value ($v > 95.0$ V) the dynamics of the system is periodic for higher f values ($f \ge 13.5$ Hz). In Fig. 4b, for low m_p values < 1.5 kg and v values in the region $0 \le v \le 115.0$ V, the system oscillates with period-1T. However, it exhibits period-3T and quasi-periodicity motion within a very narrow v region. When m_p increases ($m_p > 1.5$ kg) and $v \le 90.0$ V, the transition from periodic to chaos occurs. As m_p increases further ($m_p > 4.0$ kg), the transition from chaos to periodic oscillations takes place. As $4.5 \le m_p \le 5.0$ kg and $0 \le v \le 60.0$ V, the system exhibits period-nT ($2 \le n \le 3$) and then the transition from period-nT ($6 \le n \le 7$) to chaotic motions takes place for $v > 60.0$ V.

In Fig. 5, the bifurcation diagram (see Fig. 5a) is plotted in terms of the displacement x and the control parameter is the mass m_p of the plate at fixed parameter v. As m_p increases from 0 to 1.725 kg, the device exhibits period-1 oscillation. As m_p increases further, a sudden transition to chaos occurs leading to a first chaotic window from m_p=2.95 to 3.125 kg where chaos disappears and appears through period division and doubling sequences, respectively. Chaos reappears for m_p=3.15–4.275 kg and leads to period-1 at m_p=4.3 kg. We note, however, that this is just an example of transitions that can differ if one changes the values of the system parameters.

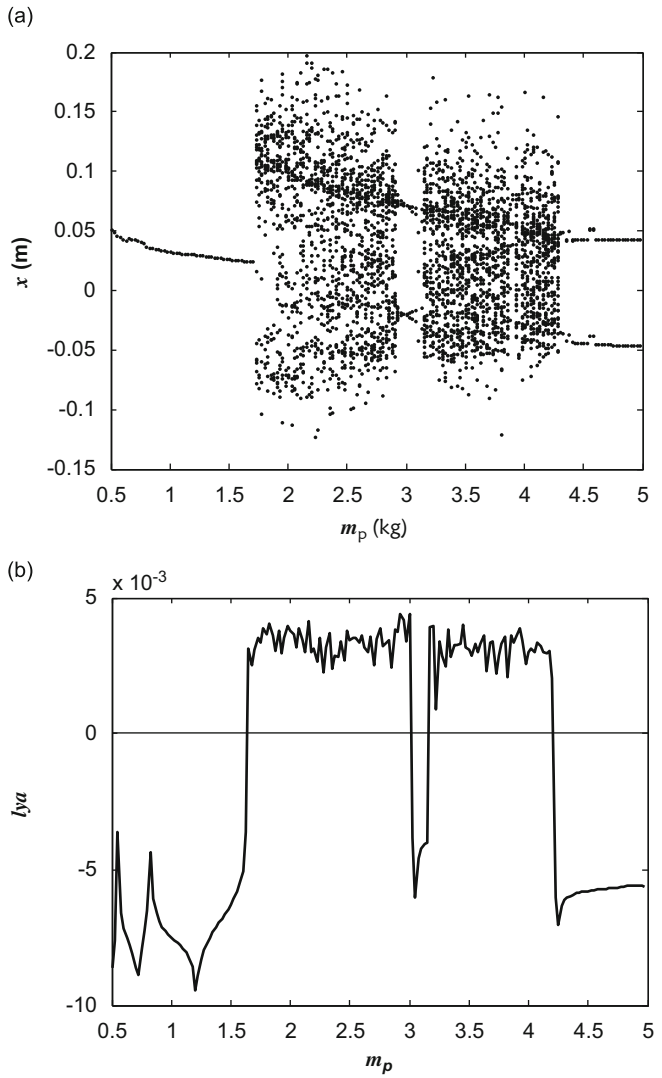

Fig. 5. (a) Bifurcation diagram and (b) Lyapunov exponent diagram, against m_p with the parameters of Fig. 4 and v=35.0 V, f=50 Hz.

Those behaviors are confirmed in Fig. 5b showing the variation of the Lyapunov exponent against m_p at fixed parameter v. The Lyapunov exponent is defined here as

$$Lya = \lim_{\tau \to \infty} \frac{\ln(\Delta(\tau))}{\tau} \tag{18}$$

where $\Delta(\tau) = \sqrt{\Delta y_1^2 + \Delta y_2^2 + \Delta \Phi_1^2 + \Delta \Phi_2^2 + \Delta \theta^2 + \Delta \Omega^2 + \Delta \dot{z}^2 + \Delta z^2}$

This figure shows chaos for $1.725 < m_p < 2.95$ kg and $3.15 \leq m_p \leq 4.3$ kg. Fig. 6 shows different phase portraits of the plate motion plotted for different steady states.

4. Anticontrol of chaos

From Section 3, numerical simulations show that, for certain values of control parameters, the system does not exhibit chaotic motions. The aim of this section is to generate desired chaos in the system independently of its intrinsic parameter values. Anti-control is done here using the field-oriented control (FOC) associated to the time delay feedback control. This consists of controlling the stator currents represented by a vector. This control is based on projections which transform a three-phase time and speed dependent system into a two coordinates (d and q-coordinates) time invariant system. These projections lead to a structure similar to that of a DC machine control. As field orientated control is based on projections, the control structure handles instantaneous electrical quantities. This makes the control accurate in every working operation (steady state and transient) and independent of the limited bandwidth mathematical model. Field orientated

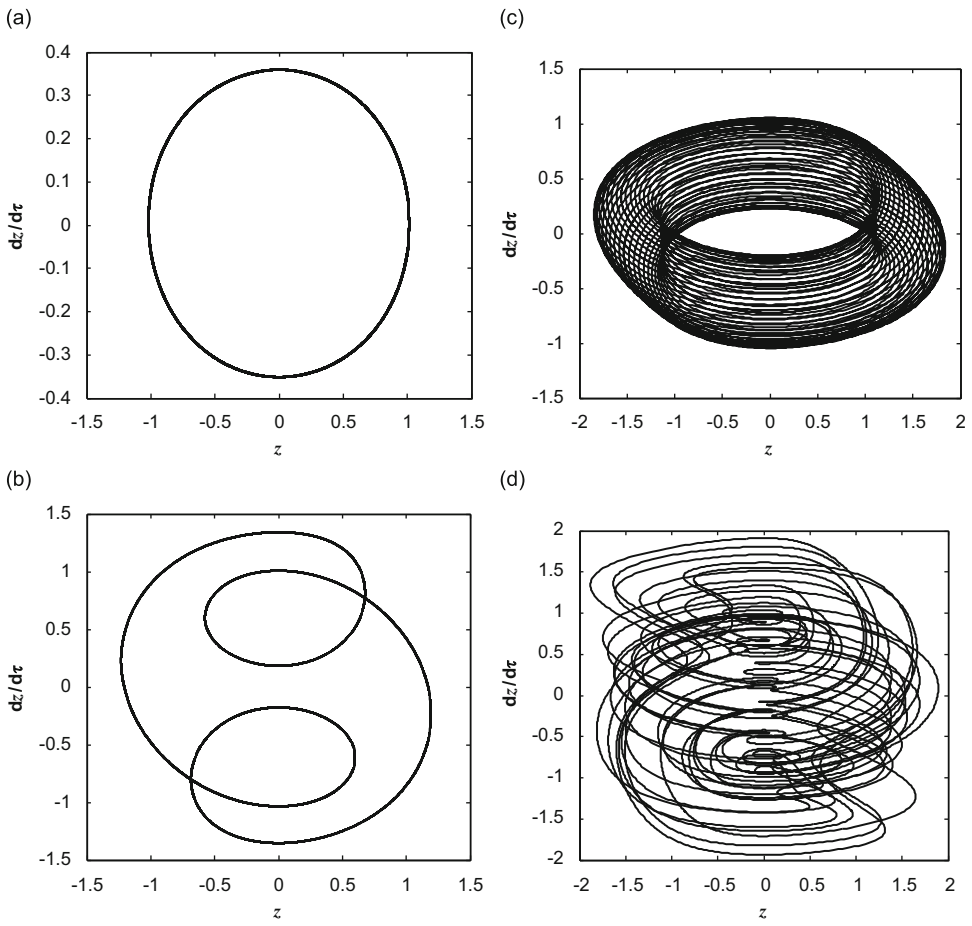

Fig. 6. Phase portraits diagrams of $(z,\dot{z})$ plane with the parameters of Fig. 4. (a) m_p=1.0 kg, f=50 Hz and v=50 v, (b) m_p=2.0 kg, f=5.5 Hz and v=62.5 V, (c) m_p=0.5 kg, f=50 Hz and v=112 V and (d) m_p=2.0 kg, f=30.0 Hz and v=25.0 V.

controlled machines need two constants as input references: the torque component (aligned with the q-coordinate) and the flux component (aligned with d-coordinate). Hence, the q-axis rotor flux becomes zero [2,4,31] and Eq. (6d) gives

$$\omega_s = n_p\omega + \frac{L_{sr} i_{sq}}{T_r \phi_{rq}} \tag{19}$$

Consider the following feedback nonlinear state where u_d and u_q are auxiliary control input voltages [2]:

$$u_{sd} = -\frac{L_{sr}}{T_r L_r}\phi_{rd} - n_p \sigma L_s \omega i_{sq} - \frac{L_{sr}}{T_r}\frac{i_{sq}^2}{\phi_{rd}}\sigma L_s + u_d \tag{20a}$$

$$u_{sq} = n_p\omega\frac{L_{sr}}{L_r}\phi_{rd} + n_p\omega\sigma L_s i_{sd} + \frac{L_{sr}}{T_r}\frac{i_{sd} i_{sq}}{\phi_{rd}}\sigma L_s + u_q \tag{20b}$$

Replacing Eq. (19) into Eqs. (17) and taking into account Eq. (20), one obtains a simple subsystem with the dynamics of the module of linear flux [2]:

$$\frac{\mathrm{d}i_{sd}}{\mathrm{d}t} + \gamma i_{sd} = \xi \cdot u_d \tag{21a}$$

$$\frac{\mathrm{d}\phi_{rd}}{\mathrm{d}t} + \frac{1}{T_r}\phi_{rd} = \frac{L_{sr}}{T_r} i_{sd} \tag{21b}$$

where the constant $\xi = 1/\sigma L_s$. One can control the dynamics of the amplitude of the flux by u_d via the proportional-integral (PI) regulators $H(s)$ shown in Figs. 7a and b with [5,32]

$$H(s) = k_p + k_I/s \tag{22a}$$

$$i_{sd}^* = H_1(s)(\phi_{ref} - \phi_{rd}) \tag{22b}$$

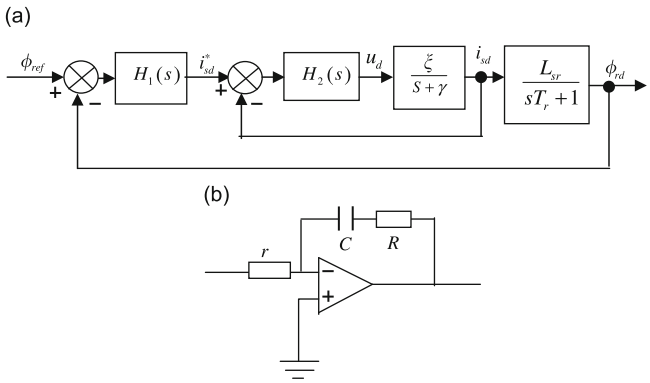

Fig. 7. (a) Flux diagram regulation and (b) PI regulator.

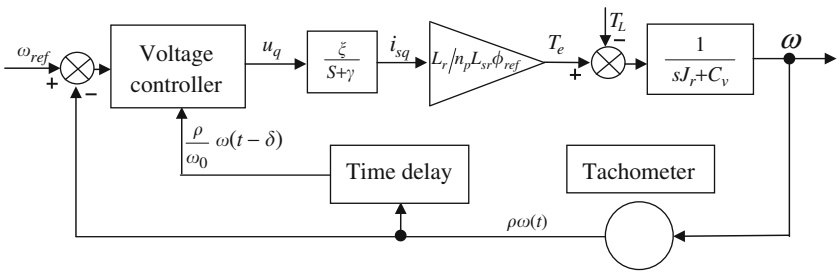

Fig. 8. Control system.

$$u_d = H_2(s)(i^*_{sd} - i_{sd}) \tag{22c}$$

where i^*_{sd} and ϕ_{ref} represent respectively the reference stator current and the reference rotor flux, in the d-axis. When the amplitude of the rotor flux ϕ_{rd} reaches its reference, which is constant, the dynamics rotor speed becomes linear too. The following second subsystem is:

$$\frac{\mathrm{d}i_{sq}}{\mathrm{d}t} + \gamma i_{sq} = \xi \cdot u_q \tag{23a}$$

$$J_r \frac{\mathrm{d}\omega}{\mathrm{d}t} + C_v\omega = n_p \frac{L_{sr}}{L_r}\phi_{ref} i_{sq} + T_L \tag{23b}$$

Eq. (23) can model the PMDC motors systems [27] where in this particular case, u_q represents the DC input voltage. To generate the desired chaos in this subsystem, one can take u_q as a controlled auxiliary excitation obtained using the time delay feedback control [33]. Fig. 8 shows the block diagram of the proposed control system.

Hence, the controlled auxiliary excitation on the q-axis can be expressed as

$$u_q = u_0 \sin\left(\frac{\rho}{\omega_0}\omega(t-\delta)\right) + (\omega_{ref} - \rho\omega) \tag{24}$$

where δ is the time delay parameter, ρ the proportional constant of the mechanical velocity, ω_{ref} is the mechanical velocity reference and u_0 the amplitude of the controlled excitation. Therefore, Eqs. (23) and (17g) give, taking into account Eq. (24)

$$\dot{y}_2 + a_1 y_2 = u\sin(\rho\Omega(\tau-\delta)) + (\Omega_{ref} - \rho\Omega) \tag{25a}$$

$$\dot{\theta} = n_p\Omega \tag{25b}$$

$$\dot{\Omega} + \mu\Omega = \chi_T \Phi_{ref} y_2 - (\eta_1\dot{z} + \eta_2 z)\frac{\cos\theta}{1-\varepsilon\sin\theta} \tag{25c}$$

$$\ddot{z} + \eta\dot{z} + z - n_p\eta\Omega\cos\theta - \sin\theta = 0 \tag{25d}$$

where $\Omega_{ref} = \omega_{ref}/\omega_0$ is the dimensionless mechanical velocity reference, Φ_{ref} the dimensionless flux reference and $u = u_0/\sigma L_s\omega_0 i_0$ the dimensionless amplitude of the controlled excitation. The set of Eq. (25) is solved numerically using the Runge–Kutta algorithm to mark the region where the system appears chaotic. This appears in the phase diagram plotted in the $\rho - u$ plane (see Fig. 9). One finds that the device exhibits chaotic motion and period-nT oscillations. At fixed value of the delay

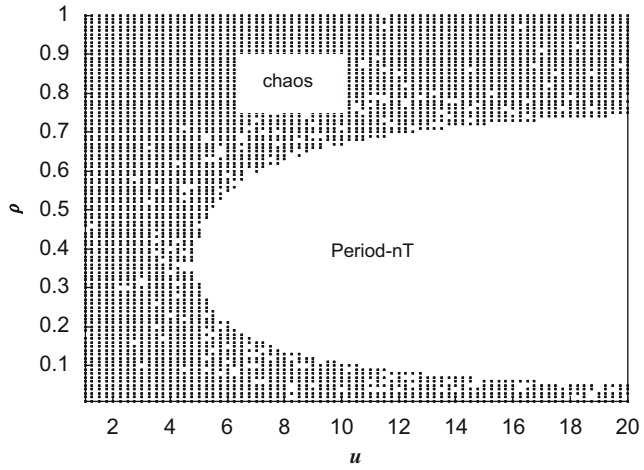

Fig. 9. Types of behaviors exhibited by the plate with the parameters of Fig. 3 and δ=1, 0 s, Φ_{ref}=0.5, Ω_{ref}=1.0.

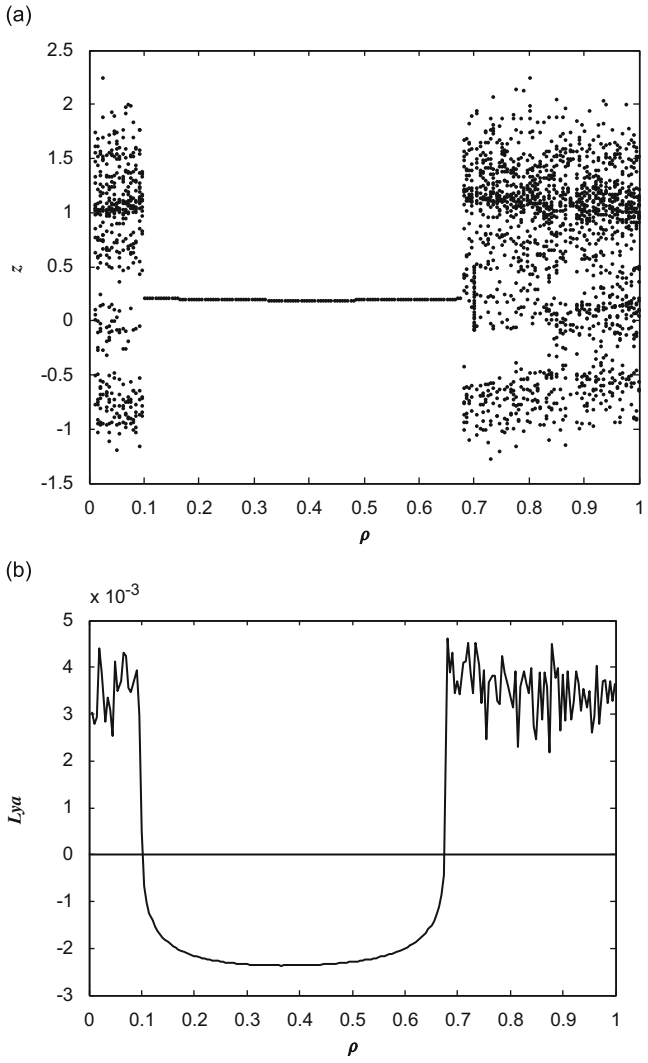

Fig. 10. (a) Bifurcation diagram and (b) Lyapunov exponent diagram, against ρ with the parameters of Fig. 9 and u=10.75.

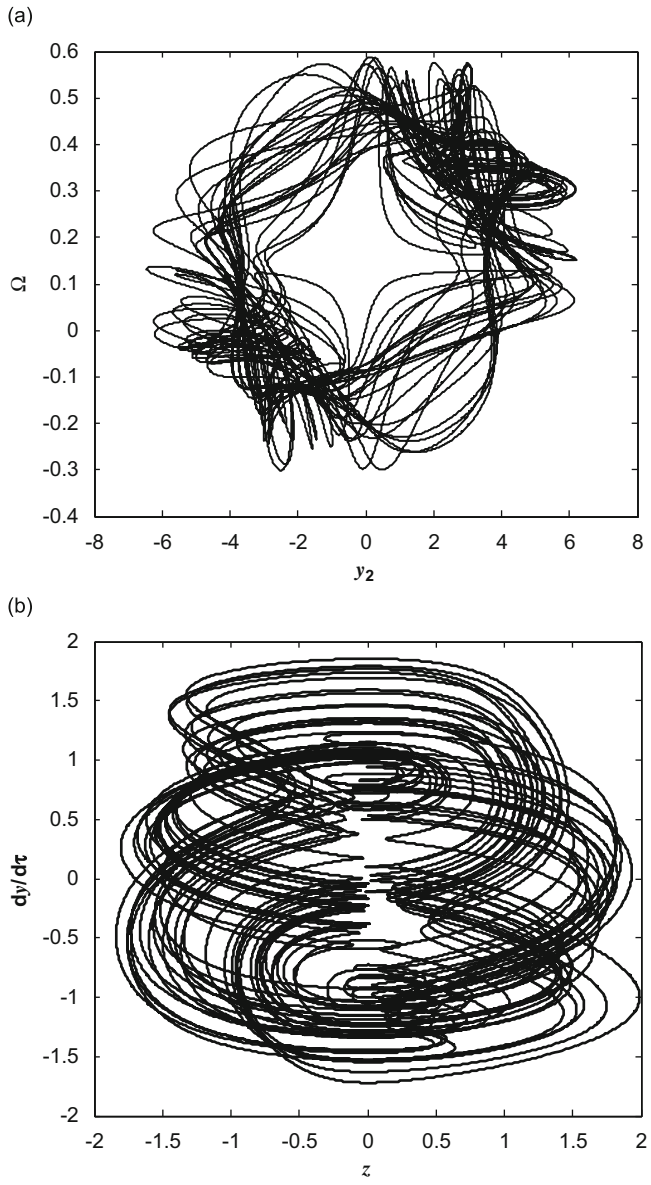

Fig. 11. (a) Electromechanical diagram of $y_2-\Omega$ and (b) phase portrait diagram of $(z,\dot{z})$ plane, with the parameters of Fig. 11 and $\rho=0.05$.

($\delta=1.0$ s), for low ρ in the range $0.0\le\rho\le1$ and u values in the range $0.1\le u\le20.0$, the device exhibits chaotic motion. As $0.1<\rho\le0.75$ and $0.1\le u\le5.0$, the device appears chaotic and then exhibits period-nT oscillation when u is varied from 5.05 to 20.0. As ρ increases further ($\rho>0.75$), the system exhibits chaotic motion for any value of the parameter u.

In Fig. 10, the bifurcation diagram (see Fig. 10a) is plotted in terms of the dimensionless displacement z and the control parameter is the proportional constant of the mechanical velocity ρ at fixed parameter u. It appears the sudden disappearance and appearance of chaos as ρ varies.

These behaviors are confirmed in Fig. 10b showing the variation of the Lyapunov exponent against ρ at the fixed parameter u. Chaos is thus present for $0\le\rho\le0.1$ and $0.68\le\rho\le1$.

Fig. 11 shows the phase portraits of the plate motion and the electromechanical diagram of AS motor plotted in one chaotic region.

5. Conclusion

In this paper, we have considered the dynamics and anti-control of chaos of an electromechanical device consisting of an induction motor which activates a mobile plate with variable contents fixed to a spring. The numerical results show

complex dynamical behaviors such as jump phenomenon, period-n motion, quasi-periodicity and chaos. Anti-control of chaos of the induction motor has been made using the field-oriented control associated to the time delay feedback control to generate the desired chaos in that device.

These results are interesting since they give the parameter ranges where the devices can be used either in the regular dynamics or in the chaotic states. Although most of the applications indicated in the introduction are presently functioning in the oscillatory state, the case of chaos is also of interest if one gets in mind that many researches are conducted nowadays with the ultimate goal of using chaotic dynamics to improve the efficiency of various robots activities such as mixing, sieving, sifting and shaking. In that spirit, one uses electromechanical, electrical and mechanical nonlinear components to design and fabricate high chaotic power mixers, sieves, sifters and shakers. However, the efficiency of this idea will be fully developed only after an experimental study to corroborate the theoretical finding and comparison with the rate of devices working periodically.

Acknowledgment

This work is supported by the Academy of Sciences for the Developing World (TWAS) under Research Grant no. 08-032 LDC/PHYS/AF/AC-UNESCO FR: 3240204452.

References

[1] M.F. Mimouni, M.N. Mansouri, B. Benghamen, M. Annabi, Vectorial command of an asynchronous motor fed by a photovoltaic generator, *Renewable Energy* 29 (2004) 433–442.
[2] A. Mansouri, M. Chenafa, A. Bouhenna, E. Etien, Powerful nonlinear observer associated with field-oriented control of an induction motor, *International Journal of Applied Mathematics and Computer Sciences* 14 (2004) 209–220.
[3] M. Ouhrouche, R. Beguenane, A.M. Trzynadlowski, J.S. Thongam, M. Dube-Dallaire, A PC-cluster based fully digital real-time simulation of a field oriented speed controller for an induction motor, *International Journal of Modeling and Simulation* 26 (2006) 219–228.
[4] A. Merabet, Commande non linéaire à modèle prédictif pour une machine asynchrone, Doctorat en Ingénierie, Université du Québec à Chicoutimi, Canada, 2007. (Model of predictive nonlinear command for asynchronous motor, Doctorate in Engineering, University of Quebec, Chicoutimi, Canada, 2007).
[5] R. Marino, S. Peresada, P. Valigi, Adaptive input–output linearizing control of induction motors, *IEEE Transactions on Automatic Control* 38 (1993) 208–221.
[6] T.K. Boukas, T.G. Habetler, High-performance induction motor speed control using exact feedback linearization with state and state derivative feedback, *IEEE Transactions on Power Electronics* 19 (2004) 1022–1028.
[7] M.K. Maaziz, P. Boucher, D. Dumur, A new control strategy for induction motor based on nonlinear predictive control and feedback linearization, *International Journal of Adaptive Control and Signal Processing* 14 (2000) 313–329.
[8] D.L. Sobczuk, Feedback linearization control of inverter fed induction motor—DSP implementation, *IEEE International Symposium on Industrial Electronics* 2 (2002) 678–682.
[9] I. Takahashi, T. Noguchi, A new quick-response and high-efficiency control strategy of an induction motor, *IEEE Transactions on Industry Applications* 22 (1986) 820–827.
[10] S.-C. Chang, P.-C. Tung, Identification of a nonlinear electromagnetic system: an experimental study, *Journal of Sound and Vibration* 214 (1998) 853–871.
[11] S.-C. Chang, H.-P. Lin, Nonlinear dynamics and chaos control for an electromagnetic system, *Journal of Sound and Vibration* 279 (2005) 327–344.
[12] D. Belato, H.I. Weber, J.M. Balthazar, D.T. Mook, Chaotic vibrations of nonideal electromechanical system, *International Journal of Solids and Structures* 38 (2001) 1699–1706.
[13] J. Awrejcewicz, Yu. Pyryev, Influence of tribological processes on a chaotic motion of a bush in a cylinder–bush system, *Meccanica* 38 (2003) 749–761.
[14] Y. Gao, K.T. Chau, Design of permanent magnets to avoid chaos in doubly salient PM machines, *IEEE Transactions on Magnetics* 40 (2004) 3048–3050.
[15] N.N. Verichev, S.N. Verichev, V.I. Erofeyev, Chaotic dynamics of simple vibrational systems, *Journal of Sound and Vibration* 310 (2008) 755–767.
[16] Z.-M. Ge, J.-M. Cheng, Y.-S. Chen, Chaos anticontrol and synchronization of three time scales brushless DC motor system, *Chaos, Solitons and Fractals* 22 (2004) 1165–1182.
[17] Z.-M. Ge, C.-I. Lee, Control, anticontrol and synchronization of chaos for an autonomous rotational machine system with time-delay, *Chaos, Solitons and Fractals* 22 (2005) 1855–1864.
[18] A. EL-Gohary, Optimal control of rigid body motion with the help of rotors using stereographic coordinates, *Chaos, Solitons and Fractals* 25 (2005) 1229–1244.
[19] Z.-M. Ge, C.-M. Chen, Y.-S. Chang, Anticontrol of chaos of single time scale brushless DC motors and chaos synchronization of different order system, *Chaos, Solitons, and Fractals* 27 (2006) 1298–1315.
[20] X.F. Wang, G. Chen, X. Yu, Anticontrol of chaos in continuous-time systems via time delay feedback, *Chaos* 10 (2000) 771–779.
[21] J.L.P. Felix, J.M. Balthazar, Comments on a nonideal electromechanical damping vibration absorber, Sommerfeld effect and energy transfer, *Nonlinear Dynamics* 55 (2009) 1–11.
[22] R. Yamapi, P. Woafo, Nonlinear electromechanical devices: dynamics and synchronization, in: R.C. Sapri (Ed.), *Mechanical Vibrations: Measurement, Effects and Control*, Nova Publishers, New York, 2009.
[23] C.A. Kitio Kwuimy, P. Woafo, Dynamics of a self-sustained electromechanical system with flexible arm and cubic coupling, *Communication in Nonlinear Science and Numerical Simulation* 12 (2007) 1504–1517.
[24] C.A. Kitio Kwuimy, Theoretical and Experimental Studies of the Dynamics of Nonlinear Electromechanical Systems with Flexible Arms, Ph.D. Thesis, Faculty of Science, University of Yaoundé 1, Cameroon, 2008.
[25] J. Jerrelind, A. Stensson, Nonlinear dynamics of parts in engineering systems, *Chaos, Solitons and Fractals* 11 (2000) 2413–2428.
[26] A. Jönsson, Lean Prototyping of Multi-body and Mechatronic Systems, Ph.D. Thesis, Department of Mechanical Engineering, School of Engineering, Karlskrona, Sweden, 2004.
[27] Z. Wang, K.T. Chau, Anti-control of chaos of a permanent magnet DC motor system for vibratory compactors, *Chaos, Solitons and Fractals* 36 (2008) 694–708.
[28] J.M. Ottino, F.J. Muzzio, M. Tjahjadi, Chaos, symmetry, and self-similarity: exploiting order and disorder in mixing process, *Science* 257 (1992) 754–760.
[29] K.T. Chau, S. Ye, Y. Gao, Application of chaotic-motion motors to industrial mixing processes, *IEEE-IAS* (2004) 1874–1880.

[30] D. Belato, A note about the appearance of non-hyperbolic solutions in a mechanical pendulum system, *Nonlinear Dynamics* 34 (2003) 309–317.
[31] J.-P. Caron, J.-P. Hautier, *Modélisation et commande de la machine asynchrone*, Collection Méthodes et Pratiques de l'Ingénieur, Edition Technip, Paris, 1995. (Modeling and command of the asynchronous motor. Methods collection and Engineer's Practical, Technip Edition, Paris, 1995).
[32] T. Van Raumer, J.M. Dion, L. Dugard, J.L. Thomas, Applied nonlinear control of an induction motor using digital signal processing, *IEEE Transactions on Control Systems Technology* 2 (1994) 327–335.
[33] Y. Gao, K.T. Chau, Chaotification of permanent-magnet synchronous motors drives using time-delay feedback, *IEEE* 1 (2002) 762–766.